Logistic regression analysis of sex-related morphological and dimensional variations of maxillary bone: a cone-beam computed tomography-based retrospective study

Santiago Palacio-Gutiérrez[1], Sara Morales-Galeano[1], Jorge L. Obando-Castillo[2], Clara I. Saldarriaga-Naranjo[3], Sergio I. Tobón-Arroyave[1]

[1] Graduate Oral and Maxillofacial Surgery Program, Faculty of Dentistry, University of Antioquia. Medellín, Colombia

[2] Department of Radiology, Cooperative University of Colombia, San Juan de Pasto, Colombia

[3] Department of Radiology, CES University and RADEX 3D Specialized Radiology Center. Medellín, Colombia

SUMMARY

This study aimed to determine, using a retrospective cone beam computed tomography (CBCT) assessment and a logistic regression analysis, which variations of the maxillary structures of interest in surgical, forensic, and anthropological practices might be linked to the sex trait in a representative sample of Colombian adults with different age and alveolar process status categories. A total of 208 CBCT scans obtained from 83 males and 125 females were evaluated. The protocol included the assessment of 40 parameters, of which 25 were bilateral and 15 were unique. The strength of association between the study variables and the sex of the individuals was examined individually and adjusted for confounding using univariate and multivariate binary logistic regression models. Although the age and alveolar process status had a confounding influence on the results, posterior maxillary region-related variables including maxillary sinus, infraorbital foramen, and greater palatine canal dimensions, but also anterior maxilla/upper middle line-related variables comprising nasopalatine canal length, anterior buccal bone thickness, and incisive foramen diameter, revealed higher values in males and remained strongly and independently associated with the male sex after adjusting for confounders. It was concluded that the maxillary bone can present several morphological variations, as well as dimensional differences that may be strongly liaised to sex, but are independent of age, side, and the state of the alveolar process of the population observed. Even so, both aging and alveolar process status should be considered when applying the anatomical variation data to the needs of the particular case.

Key words: Anatomy – Cone beam computed tomography – Maxillary bone – Retrospective studies – Sex characteristics

Corresponding author:
Sergio Iván Tobón-Arroyave, Laboratory of Immunodetection and Bioanalysis, Faculty of Dentistry, University of Antioquia, Calle 70 N° 52-21, Medellín, Colombia. Phone: (604) 2196735. E-mail: stobonarroyave@gmail.com / sergio.tobon@udea.edu.co

Submitted: March 11, 2023. **Accepted:** June 16, 2023

https://doi.org/10.52083/WQSJ7197

INTRODUCTION

Accurate knowledge of the anatomical characteristics and their variants is important for the timely diagnosis and successful treatment of the alterations of the maxillofacial region, as it allows the preservation of the integrity of morphological features and the minimization of risk of complications such as neurosensitive disorders, disruption of the cortical bone, hemorrhagic accidents, as well as nasal/sinus perforations related with improper or unsafe procedures and/or misdiagnosis (Güncü et al., 2011). For this purpose, although two-dimensional imaging methods including intra- and extra-oral radiographs have been commonly used, problems such as the overlapping, radiographic noise, magnification, and geometric distortion might make them insufficient for the detection of anatomical variants (Hakbilen and Magat, 2018) when performing oral and maxillofacial surgical interventions, thus leading to a deficient assessment and a possible iatrogenic injury. In contrast, three-dimensional methods, such as cone beam computed tomography (CBCT), allow the detailed evaluation of the configuration and exact location of the anatomical structures in the maxillofacial region (Genç et al., 2018; Hakbilen and Magat, 2018).

Compelling evidence has addressed the ability of CBCT images to characterize the alveolar process morphology (Canger and Celenk, 2012; Hakbilen and Magat, 2018; Manzanera et al., 2018) and to determine the variations in the morphological and morphometric characteristics of the maxillary sinus (MS) and accompanying anatomical structures (Genç et al., 2018; Güncü et al., 2011; Kanthem et al., 2015; Khojastehpour et al., 2016; Sahlstrand-Johnson et al., 2011; Talo Yildirim et al., 2017), infraorbital foramen (IOF) and accessory infraorbital foramen (AIOF) (Ali et al., 2018; Bahşi et al., 2019a; Dagistan et al., 2017; Martins-Júnior et al., 2017; Nanayakkara et al., 2016; Polo et al., 2019), greater palatine canal (GPC) and greater palatine foramen (GPF) (Aoun et al., 2015; Bahşi et al., 2019b; Ikuta et al., 2013; Rapado- González et al., 2015), nasopalatine canal (NPC) (Bahşi et al., 2019c; Hakbilen and Magat, 2018; Jayasinghe et al., 2020; Khojastepour et al., 2017), midpalatal suture (MPS) (Angelieri et al., 2013; Angelieri et al., 2015; Angelieri et al., 2017; Reis et al., 2020), as well as to detect incidental findings (Lopes et al., 2017; Price et al., 2012) particularly important in the surgical planning process. In spite of the acknowledged advantages of CBCT in the evaluation of these structures, all the studies available so far have only examined the effect of individual variables on their anatomical characteristics, concluding that certain parameters, including age (Genç et al., 2018; Hakbilen and Magat, 2018; Khojastepour et al., 2017), sex (Aoun et al., 2015; Bahşi et al., 2019a; Ikuta et al., 2013; Kanthem et al., 2015; Rapado-González et al., 2015; Sahlstrand- Johnson et al., 2011), and alveolar process status (Canger and Celenk, 2012; Hakbilen and Magat, 2018; Rapado-González et al., 2015), may significantly modify the morphology and dimensions of mature maxilla. Notwithstanding, research data in this field have not only been inconsistent, but also have not provided information concerning those covariables that could influence the variations as potential confounders, so that it is not possible to draw firm conclusions.

Given that the dimensional and morphological characteristics of the maxillary bone are highly variable among populations and even within the same individual, this study aimed to comprehensively determine, through a CBCT analysis, which variations of the maxillary structures of interest in the surgical, forensic, and anthropological practices could be linked to the sexual trait in a representative sample of Colombian adults with different age and alveolar process status categories.

MATERIALS AND METHODS

Study design and setting

This cross-sectional observational study was approved by the Institutional Ethics Committee for Human Studies of the University of Antioquia (Concept Number 62-2020), and was conducted following the ethical guidelines of the Helsinki Declaration on CBCT scans of patients attending a private imaging specialized center (RADEX 3D Specialized Radiology Center) in Medellín, Colombia. The sample size was calculated on the basis of patientpopulation referred for radiological exam-

ination, with a range of indications such as dental implants, endodontic procedures, orthodontics, oral diseases, and oral or periodontal surgery between January 2020 and April of 2021. Considering a total of 358 referred patients for maxillary CBCT scans, the sample size calculation using a web-based program (Raosoft® Inc., Seattle, WA, USA) indicated a sample size requirement of at least 186 digital imaging and communications of medicine (DICOM) files to identify significant variations in the bivariate comparisons with a 95% confidence level and an alpha value of 5%. However, to improve the statistical power, the study sample was increased by 22 DICOM files, which resulted in the definite inclusion of 208 maxillary scans. The inclusion criteria were patients aged over or equal to 18 years and with absence of pathological changes or traumatic and congenital deformities in the maxillary bone. On the contrary, the exclusion criteria were the low quality of CBCT images, limited field of view hindering the visualization of the full maxillary anatomy, as well as evidence of ongoing orthodontic treatment or maxillofacial surgery. Appropriate informed consent was taken from the patients to use the images for research purposes before performing CBCT scans.

Image acquisition and evaluation

CBCT images were obtained with the i-CAT® 17-19 system (Imaging Sciences International, Inc., Hatfield, Pennsylvania, USA) operated at 120 kVp, 37.07 mA, 26.9 seconds of exposure time, 16 cm x 13 cm of field vision, and 0.25 mm voxel size. All of CBCT scans were acquired using the Frankfort horizontal and the midfacial planes as references in order to prevent measurement bias induced by head position during image recording. The images were simultaneously analyzed, using the i-CATVision 1.9® software (Imaging Sciences International), by two Oral and Maxillofacial Surgeons (S. P-G. and S. M-G.) standardized by two qualified Maxillofacial Radiologists (C.I. S-N. and J.L O-C). The standardization was conducted through written guidelines and illustrative images of the different morphological changes and morphometric parameters to be evaluated. When discrepant information was reported between the two examiners, new assessments were conducted and further disagreements were arbitrated by a third researcher. All evaluations were performed on a computer screen under ideal light conditions, using the magnification function of the software to enlarge the images and the maximum intensity projection mode to achieve superior image performance.

Evaluated parameters in the analysis

Patient-related demographic parameters gathered from the study sample included information about sex (i.e., *male vs female*), age at the time of CBCT imaging, maxillary segment (i.e., *right posterior*, *left posterior*, or *anterior maxilla*), and the alveolar process status (i.e., *non-atrophic*, fully dentate *vs atrophic/partially-atrophic,* with totally edentulous maxillary segments or at least one extracted tooth, except third molars) (Talo Yildirim et al., 2017). Using multiplanar reconstructions, maxillary anatomical structures were analyzed separately on both sides of the posterior maxillary region and on the anterior maxilla/upper middle line as described below:

- The assessment of MS and their related anatomical structures included the measurement of maximum craniocaudal (height), anteroposterior (depth), and transversal (width) dimensions (Fig. 1a-c) (Kanthem et al., 2015). The maximum MS height was measured on coronal views as the distance between the uppermost point of the roof and the lowermost point of the floor, whereas the depth and width were measured on axial views estimating the distances among the most anterior and posterior walls and among the outermost and medial point of the MS, respectively. Then, the minimum perpendicular distance from the sinus floor to the alveolar crest (AC) was determined (Figs. 1d and e) taking as landmark the deepest point of the sinus floor within the alveolar process as observed in the panoramic and coronal cuts.
- Other parameters included in the data set were the presence/absence of antral septa (Fig. 1f and g), identified as walls of cortical bone with a minimal expansion of 2 mm in any of the orthogonal views within the MS (Hungerbühler et al., 2019); and the detec-

tion of the posterior superior alveolar artery canal (PSAAC), its greater diameter, as well as its distance to the alveolar crest (Fig. 1h-k) measured as a vertical line in the upper second molar region (Elian et al., 2005; Güncü et al., 2011; Khojastehpour et al., 2016). This PSAAC was identified as a well-defined, corticated, circular hypodensity or C-shaped curve of the lateral sinus wall and registered as *non-detected vs present* (including the intraosseous, below the membrane, or on the outer cortex presentations).

- With the purpose of analyzing the infraorbital region, the greater diameter of IOF in the three orthogonal planes, the vertical distance from the IOF to the AC (Bahşi et al., 2019a; Dagistan et al., 2017; Nanayakkara et al., 2016) (Fig. 2a-c), as well as the presence/absence of the canalis sinuosus (von Arx et al., 2013) (Csin, Fig. 2b and c) and of the AIOF (Ali et al., 2018) (Fig. 2d-f) in the anterior wall of MS were also included in the analysis.
- The morphometric evaluation of the GPC and the GPF included the measurement of the length of the GPC in the sagittal plane from the central point of the pterygopalatine fossa (PPF, superior aspect) to the central point of the GPF (inferior aspect) following established criteria (Tomaszewska et al., 2015) with modifications. The length of GPC was obtained in millimeters, considering the sum of the length of two lines intersecting in the center of the canal (Fig. 3a). Furthermore, the maximum anteroposterior diameter of the GPC in the axial plane and its distance in relation to the posterior nasal spine (PNS), the NPC, and the pterygoid hamulus (Bahşi et al., 2019b; Rapado-González et al., 2015) were measured with the sagittal palatal plane positioned through the center of the supero-inferior dimension of the hard palate (Fig. 3b). Also, for each GPF, several observations were made using axial or coronal reconstructions: *(1)* perpendicular distance from the medial wall of GPF to the midline maxillary suture (MMS, Fig. 3c) (Bahşi et al., 2019b, Ikuta et al., 2013); *(2)* perpendicular distance from the center of GPF opening to the AC (Fig. 3c); *(3)* the angle between the horizontal plane of the palatine bone and the vertical axis of the GPC measured in the coronal view (Fig. 3d); *(4)* the localization of the GPF with respect to the posterior margin of the palatine bone

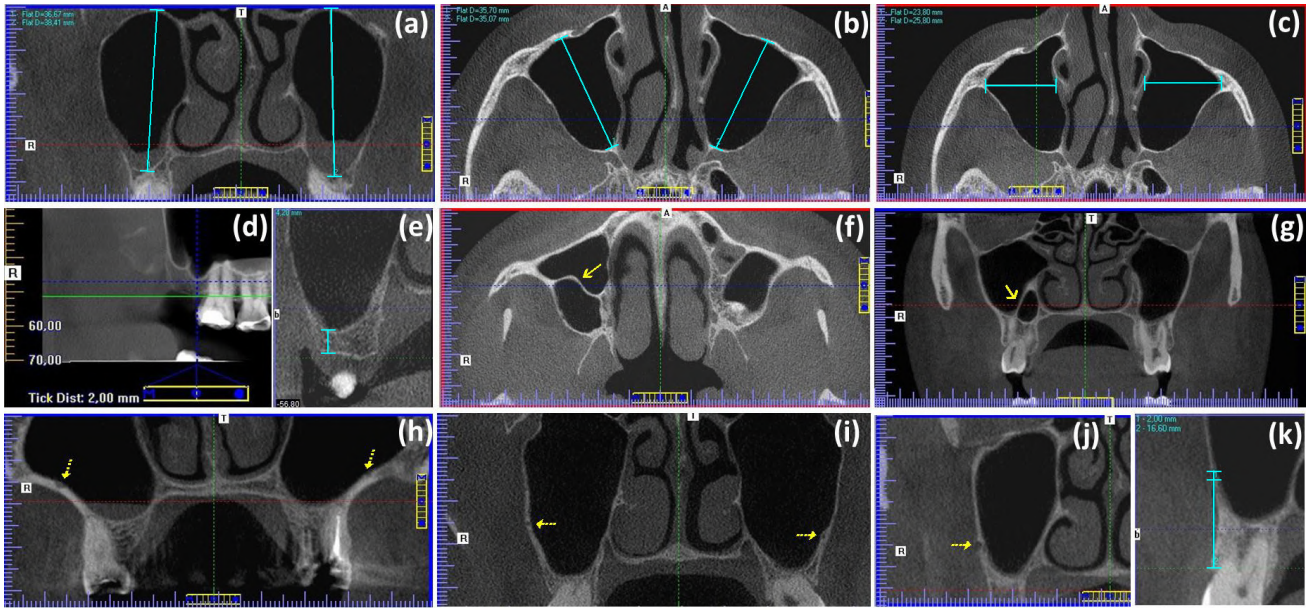

Fig. 1.- Representative CBCT scans of MS and accompanying anatomical structures. Images (a) to (e) illustrate the method of measurement (green lines) of some variables as follows: (**a**) maximum craniocaudal (height), (**b**) maximum anteroposterior (depth), and (**c**) maximum transversal (width); (**d** and **e**) minimum perpendicular distance from the sinus floor to the alveolar crest. (**f**) Axial and (**g**) coronal views demonstrating the presence of antral septa (solid arrows). Images (h) to (k) depict the anatomical location of the PSAA canal as detected through coronal sections (dotted arrows): (**h**) below the membrane, (**i**) intraosseous, and (**j**) on the outer cortex. (**i**) Measurement of the diameter of and the distance from the PSAA canal to the alveolar crest (green lines).

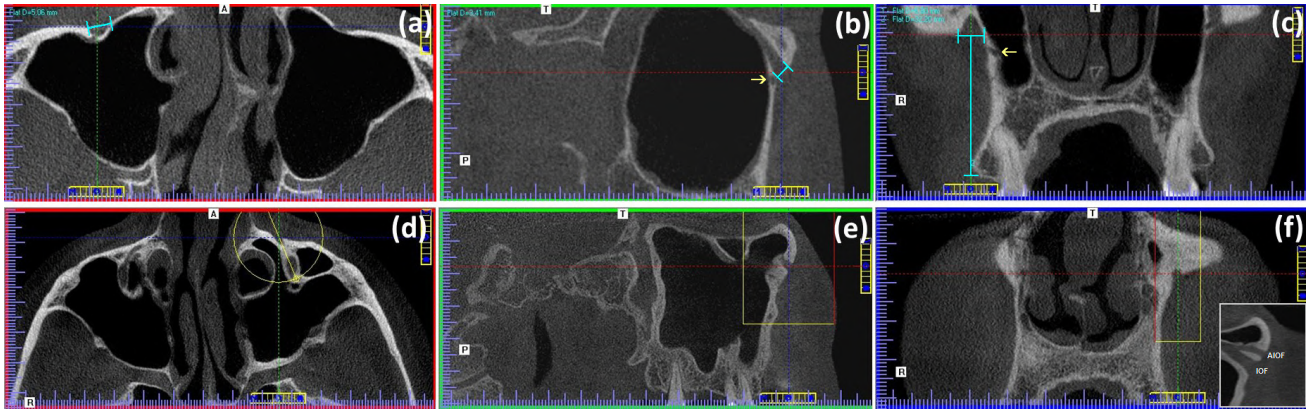

Fig. 2.- CBCT scans of the infraorbital region showing: (**a**) the greater transverse (axial) diameter of IOF, (**b**) the greater sagittal diameter of IOF and the CSin (solid arrow) within the anterior wall of the MS, and (**c**) the greater coronal diameter of IOF, the CSin (solid arrow), and the vertical distance to the crest of the alveolar bone from the mid-point of the IOF. The lower row shows the (**d**) axial, (**e**) sagittal, and (**f**) coronal sections used to view additional cut planes in order to explore the canal leading to the AIOF (inset).

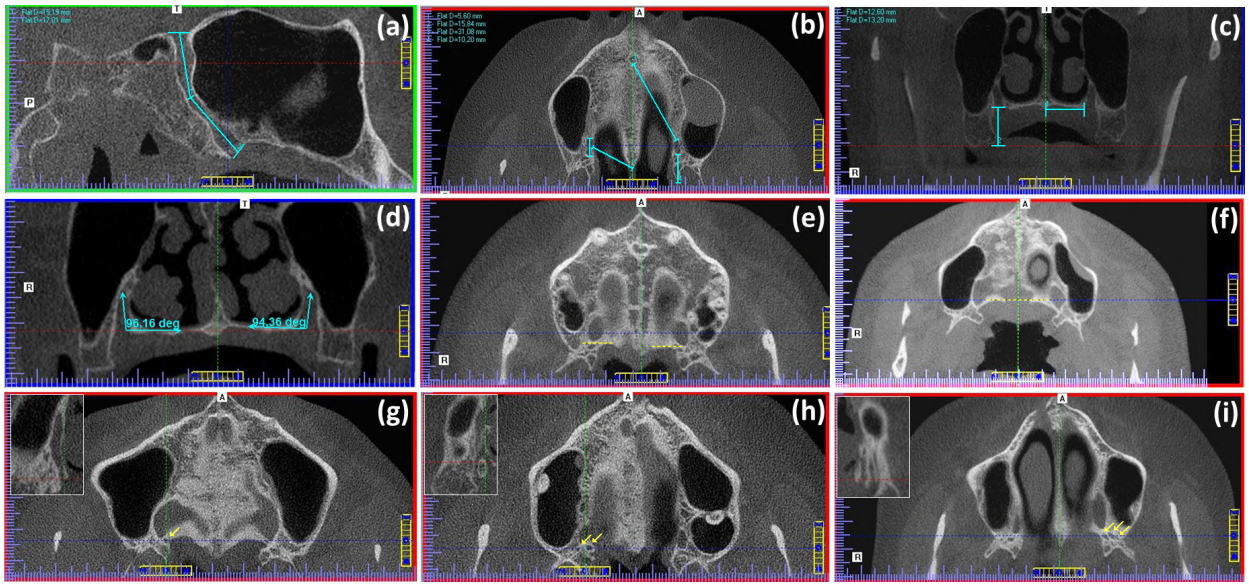

Fig. 3.- Landmarks selected to determine the position and dimensions of the GPC and the GPF in different tomographic planes. The green lines illustrate the path by which the measurements were obtained: (**a**) length of GPC in the sagittal plane; (**b**) maximum anteroposterior diameter of the GPC in the axial plane and its distance regarding the posterior nasal spine, NPC, and the pterygoid hamulus; (**c**) distance between the medial wall of GPF and the MMS and distance from the center of GPF to the alveolar crest; (**d**) angle between the horizontal plane of the palatine bone and the vertical axis of the GPC; localization anterior (**e**) and on the same line (**f**) of the GPF with reference to a tangent line to the posterior margin of the palatine bone (dashed yellow lines); (**g-i**) axial sections showing one, two, and three openings of LPF (solid yellow arrows), respectively (insets: coronal views used to determine the trajectory of the corresponding lesser palatine canals).

(i.e., *anterior vs on the same line*, Fig. 3e and f); and *(5)* the number of the lesser palatine foramina (LPF, i.e., *one vs two or more*, Fig. 3g-i) (Bahşi et al., 2019b; Gibelli et al., 2017).

- Several anatomical landmarks were assessed on the maxillary midline. In the sagittal plane, the shape of NPC was classified according to earlier descriptions (Bahşi et al., 2019c; Hakbilen and Magat, 2018; Jayasinghe et al., 2020) in several groups including *hourglass- shaped*, *cone-shaped*, *funnel-shaped*, *cylindrical*, *banana-shaped,* and *branched* (Fig. 4a-f). In addition, the form of NPC was classified in the coronal plane in three groups: *Y-shaped*, *single canal*, and *double canal* (Fig. 4g-i), whereas in the axial plane (Fig. 4o and p), the shape (i.e., *round-*, *oval-*, *triangle-*, *heart-*, or *kidney-shaped*) and number of openings (i.e., *one vs two or more*) of NPC at the mid-level, nasopalatine foramen (NPF), and incisive foramen (IF) were examined according to defined criteria

(Bahşi et al., 2019c). Alternatively, some quantitative parameters were calculated on the maxillary midline, including the anteroposterior diameters of NPF and IF, the length of NPC (Fig. 4q), measured as the distance between the midpoints of NPF and IF (Bahşi et al., 2019c, Bornstein et al., 2011; Hakbilen and Magat, 2018), the minimum anterosuperior buccal bone thickness (Fig. 4r), and the NPC angle (Fig. 4s) located anteriorly among the axis of NPC and the palatal plane (Bahşi et al., 2019c). Furthermore, MPS maturation was evaluated on the central axial view of the palate and categorized in stages A to E (Fig. 5 a-e) using validated data (Angelieri et al., 2013).

- All incidental findings defined as unexpected bone abnormalities with potential clinical significance (Price et al., 2012) such as torus palatinus (Fig. 5f), palatal/buccal exostoses (Figs. 5g and h), and idiopathic osteosclerosis (Fig. 5i), were documented for both posterior maxillary segments and the anterior maxilla/upper middle line. Conversely, findings such as dental caries, periapical/periodontal conditions, root remnants, altered tooth morphology, supernumerary teeth, and eruption disturbances were ruled out of the study.

Statistical methods

Data processing was completed in standard statistical software (SPSS, v.27.0, IBM, Armonk, NY). Several steps were carried out during the analytic process. Initially, the intra-observer variability was determined through double assessments for each parameter conducted simultaneously by the same examiners using 20 DICOM files chosen following a simple random sampling procedure. For comparisons, the reliability between the two series of data was assessed by using the Cohen's kappa (κ) or the weighted kappa (κ_w) statistics for categorical variables and the intraclass correlation coefficient (ICC) for quantitative variables. The interval between tests 1 and 2 was 12 months.

Bivariate analyses were performed to detect differences in morphological and dimensional variables regarding independent variables. For quantitative variables, the mode of distribution of the data was analyzed using the Kolmogorov-Smirnov test. Because the data were normally distributed, they were analyzed using the independent samples *t*-test. Homoscedasticity was confirmed

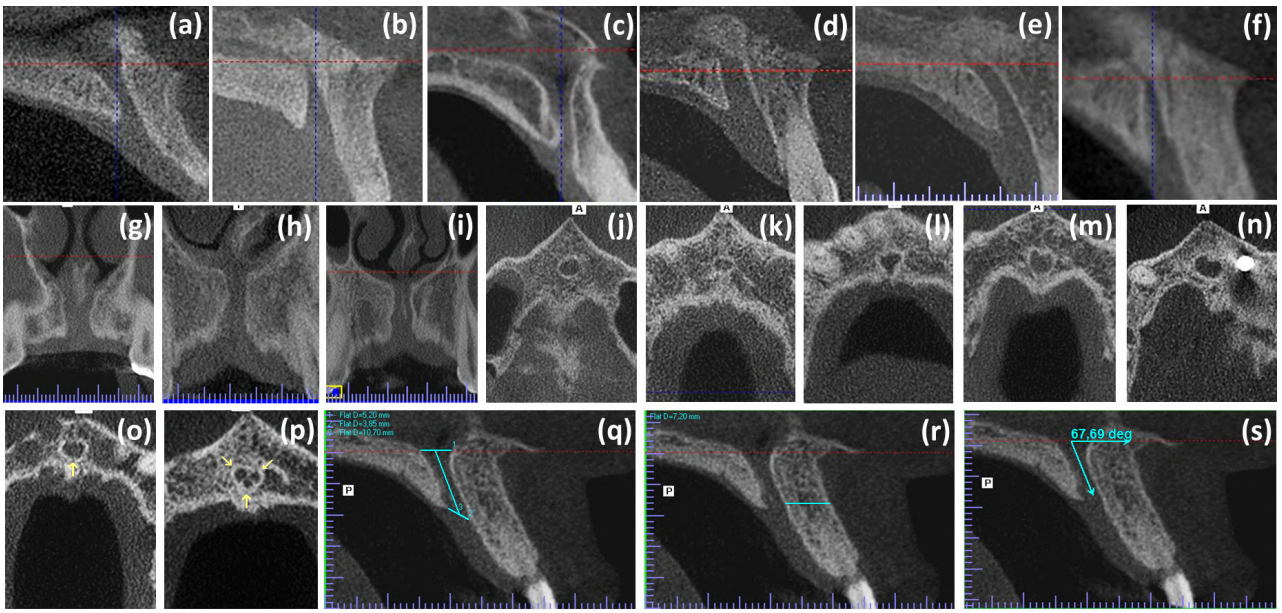

Fig. 4.- CBCT images showing morphological and dimensional evaluations of different anatomical landmarks assessed on the maxillary midline. The morphological variations of NPC were classified in the sagittal plane as: (**a**) hourglass-shaped, (**b**) cone-shaped, (**c**) funnel-shaped, (**d**) cylindrical, (**e**) banana-shaped, and (**f**) branched. In the coronal plane, the configuration of NPC was categorized as: (**g**) Y-shaped, (**h**) single canal, and (**i**) double canal. In the axial plane the shapes of NPF, IF or NPC were classified at each level as: (**j**) round-shaped, (**k**) oval-shaped, (**l**) triangle-shaped; (**m**) heart-shaped, or (**n**) kidney-shaped, whereas the number of openings was stratified as having (**o**) one and (**p**) two or more openings (solid yellow arrows). Measurements of anatomical structures in sagittal sections included (**q**) the length of the NPC and the diameters of IF and NPF, (**r**) the minimum anterosuperior buccal bone thickness, and (**s**) the NPC angle.

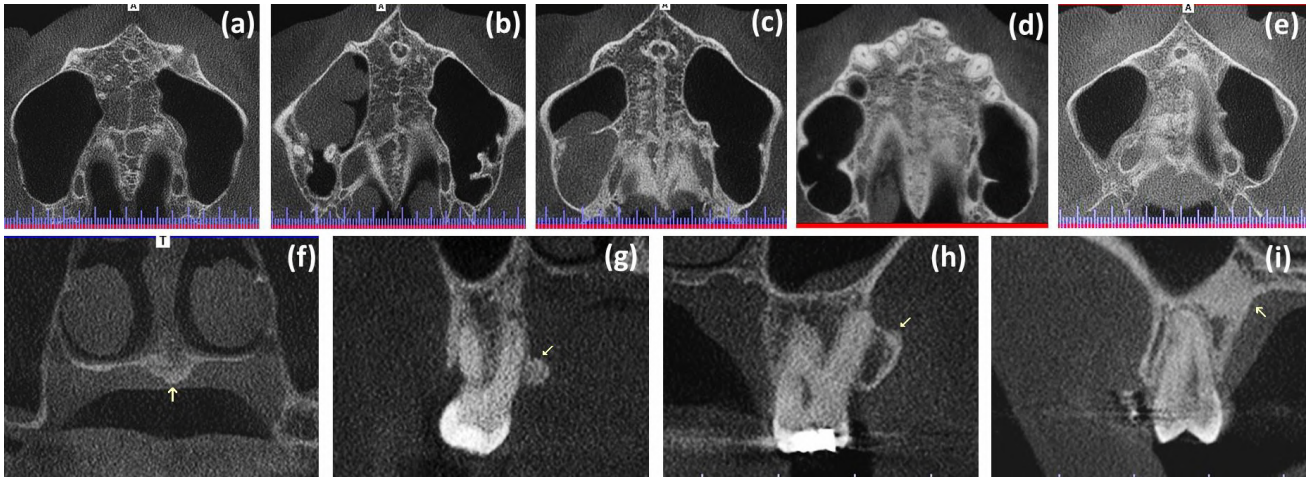

Fig. 5.- CBCT images showing maturation stages of the midpalatal suture (upper row) and some incidental findings of the maxillary region (lower row). (**a**) Stage A of maturation of the midpalatal suture seen as a unique high-density line at the midline. (**b**) Stage B of maturation identified as a scalloped high-density line in some areas and, in other areas, as two parallel, scalloped, high-density lines close to each other and separated by small low-density spaces. (**c**) Stage C of maturation visualized as two parallel, scalloped, and high-density lines separated in some areas by small low-density spaces. (**d**) Stage D of maturation visualized as two scalloped, high-density lines on the maxillary portion of the palate but not observed on the palatine bone. (**e**) Stage E of maturation in which the midpalatal suture cannot be recognized. The lower row shows magnified coronal views demonstrating the presence of (**f**) a torus palatinus in the midline of the palate (solid yellow arrow), (**g**) a palatal exostosis of the maxillary alveolar process (solid yellow arrow), (**h**) a buccal exostosis of the maxillary alveolar process (solid yellow arrow), and (**i**) the tomographic appearance of an apical idiopathic osteosclerosis (solid yellow arrow).

using Levene's test for equality of variances. Furthermore, Pearson's chi-square test (χ^2) was used to compare categorical variables.

Finally, univariate and multivariate binary logistic regression analyses were applied to confirm the association of significant candidate variables with the sex adjusting for independent confounding variables with a level of significance of P <0.20 identified in the bivariate analyses. With this purpose, all continuous data included in the regression models were dichotomized according to the optimal cut-offs points obtained from receiver operating characteristic (ROC) curve analysis. Positive associations occurred when the odds ratio (OR) was >1 and the confidence interval (CI) did not show a value of 1 on any of the constructs. In addition, the Hosmer-Lemeshow statistic was used to assess the goodness of fit of the regression models. Statistical significance was assumed at a value of P <0.05.

RESULTS

Sample characteristics and reproducibility analysis

The study included 208 DICOM files acquired from 83 males with an age range from 18 to 76 years (mean 47.02 ± 15.87) and 125 females with an age range from 18 to 86 years (mean 52.36 ± 15.57). Based on the ROC curve, for all comparisons the optimal cut-off point of the age was estimated in 50.5 years. For each DICOM file, irrespective of the sex, age, side, or alveolar process status, a total of 40 anatomical variables were gathered and analyzed. It was noteworthy that 242 (58.20%) out of 416 posterior maxillary segments were categorized as non-atrophic, 134 (32.20%) as partially atrophic, and 40 (9.60%) as atrophic. Likewise, the anterior maxillary alveolar process status was classified as non-atrophic in 140 (67.30%) out of 208 cases, partially atrophic in 49 (23.60%) cases, and atrophic in 19 (9.10%) cases. Overall, in the reproducibility analysis, the variability between the two series of data obtained by the same examiners was distributed around either the mean or the observed values, without trends towards over- or under-estimation, so that the study results did not show important differences for intra-observer reliability for any of the quantitative or for categorical parameters tested. Thus, the reliability values varied between 0.866 and 1.000, being significantly excellent (P <0.001; ICC, Cohen's κ, and κ_w tests) for all of the variables.

Bivariate comparisons of demographic and tomographic characteristics of the sample

Tables 1 and 2 display the between-group comparisons of the posterior maxillary region- or of the anterior maxilla/upper middle line-related variables regarding to the sex distribution. From Table 1 is apparent that while no significant differences (all $P > 0.05$, χ^2 or unpaired t tests) were detected between sex categories with respect to the minimum distance from the sinus floor to the AC; presence of antral septa; detection, diameter, and distance to the AC of the PSAAC; detection of Csin or AIOF; angle among the horizontal plane of PB and the GPC; localization of the GPF regarding to the posterior margin of the PB; number of the LPF; nor to incidental findings; those data regarding the maximum height, depth, and width of MS; axial, sagittal, and coronal dimensions of IOF; distance from the IOF to the AC; length of GPC in the sagittal plane; anteroposterior diameter of the GPC in the axial plane; distance from the GPC to the PNS, NPC, and to pterygoid hamulus; as well as distance of GPF to the MMS and to AC were significantly greater (all $P < 0.05$, unpaired t-test) in the male group in comparison with the female group. Conversely, both the age and the posterior alveolar process status fulfilled the condition to be deemed as independent confounding variables for the association among sex categories and the variations of maxillary anatomical structures, as they attained P- values <0.20 (χ^2 or unpaired t tests) in the bivariate tests. Otherwise, only the mean values of the length of NPC at sagittal plane, the minimum anterior-superior buccal bone thickness, and the diameter of IF were significantly higher in the male group ($P < 0.01$, unpaired t-test) when compared with the female group (Table 2), whereas the age and the anterior maxillary alveolar process status also had a confounding influence on the results ($P < 0.20$, χ^2 or unpaired t tests). Additionally, in order to identify further sources of variability, all morphological and morphometric data were evaluated by comparing with age, maxillary sides, and alveolar process status when indicated. As a result, no significant differences (all P-values >0.05, χ^2 or unpaired t tests, data not shown) could be established for any parameter of the posterior segments with respect to age and maxillary sides. On the contrary, those cases with atrophic/partially atrophic posterior alveolar processes showed significantly lesser distances from the sinus floor or from lower border of the PSAAC to the AC and a greater proportion of the GPF were located on the same line of the posterior margin of the PB (P-values <0.05, data not shown). In the same way, data of the anterior maxilla/upper middle line showed significantly decreased mean values (P-values <0.01, unpaired t test, data not shown) for both the length of NPC at sagittal plane and the minimum anterior-superior buccal bone thickness in cases with age >50.5 years and atrophic/partially atrophic alveolar process status. Moreover, cases aged >50.5 years had a significantly greater proportion ($P < 0.001$, χ^2 test, data not shown) of stage E of maturation of the MPS. Hence, these findings confirmed the confounding effect of the age and of the alveolar process status on the outcomes.

Outcomes from univariate and multivariate binary logistic regression models

The outcomes from univariate and multivariate models for the association of those variables that yielded significant differences in the bivariate analyses of both posterior maxillary region and anterior maxilla/upper middle line with the sex of the individuals, are presented in Tables 3 and 4, respectively. In general, the Hosmer-Lemeshow goodness-of-fit test values fluctuated from 0.206 to 0.994, indicating that the models were adequately adjusted. Regarding posterior maxillary region-related variables, it can be seen from Table 3, that the OR was significantly increased ($P < 0.05$, Wald's test) for male group in cases with MS height >35.65 mm, MS depth >35.44 mm, MS width >26.65 mm, diameter of IOF in the axial plane >4.15 mm, diameter of IOF in the sagittal plane >3.67 mm, diameter of IOF in the coronal plane >3.71 mm, distance from the mid-point of the IOF to the AC >29.72 mm, length of GPC in the sagittal plane >35.60 mm, anteroposterior diameter of the GPC in the axial plane >5.55 mm, distance from the GPC to the PNS >15.78 mm, distance from the GPC to the NPC >31.94 mm, distance from the GPC to the pterygoid hamulus >9.25 mm, distance from the medial wall of GPF

Table 1. Bivariate comparisons of posterior maxillary region-related variables regarding to the sex distribution.

Parameter		Sex category[a]		P-value
		Male (n = 166)	Female (n = 250)	
Age (years)[b]		47.15 ± 15.96	52.36 ± 15.44	0.001[e]
Posterior alveolar process status[c]	Non-atrophic	90 (54.20)	152 (60.80)	0.183[f]
	Atrophic/partially atrophic	76 (45.80)	98 (39.20)	
Maximum MS height (mm)[b]		39.23 ± 4.90	34.48 ± 4.23	<0.001[e]
Maximum MS depth (mm)[b]		37.35 ± 3.74	34.45 ± 3.22	<0.001[e]
Maximum MS width (mm)[b]		27.97 ± 5.08	25.80 ± 4.20	<0.001[e]
Minimum distance from the sinus floor to the AC (mm)[b]		6.25 ± 3.68	6.34 ± 3.01	0.762[e]
Antral septa[c]	Present	75 (45.20)	98 (39.20)	0.226[f]
	Absent	91 (54.80)	152 (60.80)	
Detection of PSAAC[c]	Present[d]	125 (75.30)	189 (75.60)	0.945[f]
	Non-detected	41 (24.70)	61 (24.40)	
Diameter of PSAAC (mm)[b]		1.37 ± 0.55	1.26 ± 0.44	0.060[e]
Distance among lower border of the PSAAC to the AC (mm)[b]		16.16 ± 3.76	15.90 ± 3.67	0.549[e]
Greater diameter of IOF in the axial plane (mm)[b]		4.50 ± 1.07	4.12 ± 0.92	<0.001[e]
Greater diameter of IOF in the sagittal plane (mm)[b]		3.99 ± 0.91	3.51 ± 0.86	<0.001[e]
Greater diameter of IOF in the coronal plane (mm)[b]		3.96 ± 0.81	3.59 ± 0.72	<0.001[e]
Distance from the mid-point of the IOF to the AC (mm)[b]		31.29 ± 3.29	29.69 ± 2.76	<0.001[e]
Detection of Csin[c]	Present	152 (91.60)	214 (85.60)	0.067[f]
	Absent	14 (8.40)	36 (14.40)	
AIOF[c]	Present	34 (20.50)	34 (13.60)	0.063[f]
	Absent	132 (79.50)	216 (86.40)	
Length of GPC in the sagittal plane (mm)[b]		37.58 ± 3.05	34.97 ± 3.01	<0.001[e]
Anteroposterior diameter of the GPC in the axial plane (mm)[b]		6.34 ± 1.57	5.27 ± 1.22	0.003[e]
Distance from the GPC to the PNS (mm)[b]		16.44 ± 1.29	15.33 ± 1.71	<0.001[e]
Distance from the GPC to the NPC (mm)[b]		33.11 ± 3.37	31.81 ± 3.14	<0.001[e]
Distance from the GPC to the pterygoid hamulus (mm)[b]		9.69 ± 1.68	9.00 ± 1.69	0.001[e]
Distance from the medial wall of GPF to the MMS (mm)[b]		13.87 ± 1.45	13.53 ± 1.45	0.020[e]
Distance from the center of GPF to the AC (mm)[b]		11.18 ± 2.36	9.31 ± 2.33	<0.001[e]
Angle among the horizontal plane of PB and the GPC (degrees)[b]		93.27 ± 7.76	94.41 ± 9.08	0.172[e]
Localization of the GPF regarding to the posterior margin of the PB[c]	Anterior	121 (72.90)	179 (71.60)	0.774[f]
	On the same line	45 (27.10)	71 (24.80)	
Number of the LPF[c]	One	90 (54.20)	159 (63.60)	0.056[f]
	Two or more	76 (45.80)	91 (36.40)	
Incidental findings[c]	Absent	155 (93.40)	232 (92.80)	0.242[f]
	Palatal/buccal exostoses	11 (6.60)	14 (5.60)	
	Idiopathic osteosclerosis	--	4 (1.60)	

Abbreviations: MS, maxillary sinus; AC, alveolar crest; PSAAC, posterior superior alveolar artery canal; IOF, infraorbital foramen; Csin, canalis sinuosus; AIOF, accessory infraorbital foramen; GPC, greater palatine canal; PNS, posterior nasal spine; NPC, naso-palatine canal; GPF, greater palatine foramen; MMS, midline maxillary suture; PB, palatine bone; LPF, lesser palatine foramina
[a]Data based on the sum of right- and left-maxillary posterior sides
[b]Values are given as mean ± SD
[c]Values given as n (%) of cases within each parameter according to the sex category
[d]Including intraosseous (n = 217), below the sinus membrane (n = 81), and on the outer cortex (n = 16) locations
[e]Two-sided unpaired t-test
[f]Two-sided Pearson's chi-square test (χ^2)

Table 2. Bivariate comparisons of anterior maxilla/upper middle line-related variables regarding to the sex distribution.

Parameter		Sex category		P-value
		Male (n = 83)	Female (n = 125)	
Age (years)[a]		47.02 ± 15.87	52.36 ± 15.57	0.015[c]
Anterior maxillary alveolar process status[b]	Non-atrophic	51 (61.40)	89 (71.20)	0.142[d]
	Atrophic/partially atrophic	32 (38.60)	36 (28.80)	
Sagittal morphology of NPC[b]	Hourglass-shaped	22 (26.50)	27 (21.60)	0.421[d]
	Cone-shaped	10 (12.00)	11 (8.80)	
	Funnel-shaped	15 (18.10)	22 (17.60)	
	Banana-shaped	14 (16.90)	24 (19.20)	
	Cylindrical	16 (19.30)	37 (29.60)	
	Branched	6 (7.20)	4 (3.20)	
	Y-shaped	29 (34.90)	40 (32.00)	
Coronal morphology of NPC[b]	Single canal	48 (57.80)	80 (64.00)	0.491[d]
	Double canal	6 (7.20)	5 (4.00)	
Axial mid-level morphology of NPC[b]	Round-shaped	36 (43.40)	45 (36.00)	0.302[d]
	Oval-shaped	15 (18.10)	29 (23.20)	
	Triangle-shaped	8 (9.60)	5 (4.00)	
	Heart-shaped	17 (20.50)	31 (24.80)	
	kidney-shaped	7 (8.40)	15 (12.00)	
Number of NPC at mid-level of axial plane[b]	One canal	65 (78.30)	104 (83.20)	0.377[d]
	Two or more canals	18 (21.70)	21 (16.80)	
Length of NPC at sagittal plane[a]		13.04 ± 3.02	10.93 ± 2.42	<0.001[c]
NPC angle at sagittal plane[a]		69.06 ± 8.57	67.11 ± 9.26	0.123[c]
Minimum anterior-superior buccal bone thickness[a]		7.22 ± 1.51	6.03 ± 1.71	0.001[c]
Diameter of IF[a]		4.08 ± 0.92	3.48 ± 0.96	0.001[c]
Axial morphology of IF[b]	Round-shaped	29 (34.90)	43 (34.40)	0.098[d]
	Oval-shaped	13 (15.70)	9 (7.20)	
	Triangle-shaped	18 (21.70)	24 (19.20)	
	Heart-shaped	18 (21.70)	45 (36.00)	
	kidney-shaped	5 (6.00)	4 (3.20)	
Number of IF at axial plane[b]	One opening	78 (94.00)	120 (96.00)	0.504[d]
	Two or more openings	5 (6.00)	5 (4.00)	
Diameter of NPF[a]		3.67 ± 1.82	3.41 ± 1.63	0.296[c]
Axial morphology of NPF[b]	Round-shaped	28 (33.70)	39 (31.20)	0.403[d]
	Oval-shaped	28 (33.70)	30 (24.00)	
	Triangle-shaped	4 (4.80)	6 (4.80)	
	Heart-shaped	7 (8.40)	17 (13.60)	
	kidney-shaped	16 (19.30)	33 (26.40)	
Number of NPF at axial plane[b]	One opening	46 (55.40)	85 (68.00)	0.066[d]
	Two or more openings	37 (44.60)	40 (32.00)	
MPS maturation[b]	Stage A	3 (3.60)	--	0.259[d]
	Stage B	5 (6.00)	11 (8.80)	
	Stage C	12 (14.50)	16 (12.80)	
	Stage D	17 (20.50)	24 (19.20)	
	Stage E	46 (55.40)	74 (59.20)	
Incidental findings[b]	Absent	78 (94.00)	107 (85.60)	0.059[d]
	Torus palatinus	5 (6.00)	18 (14.40)	

Abbreviations: NPC, nasopalatine canal; IF, incisive foramen; NPF, nasopalatine foramen; MPS, midpalatal suture
[a]Values are given as mean ± SD
[b]Values given as n (%) of cases within each parameter according to the sex category
[c]Two-sided unpaired t-test
[d]Two-sided Pearson's chi-square test (χ^2)

Table 3. Univariate/multivariate binary logistic regression analyses for association of significant posterior maxillary region-related variables with the sex trait adjusting for age and alveolar process status.

Parameters		Cases[a]		Univariate analysis		Multivariate binary logistic regression analysis		Calibration[d]
		Male (n = 166)	Female (n = 250)	Unadjusted OR (95% CI)[b]	P-value[c]	Adjusted OR (95% CI)[b]	P-value[c]	
MS height	≤35.65 mm	36 (21.70)	155 (62.00)	Referent	<0.001	5.94 (3.77 – 9.35)	<0.001	0.206
	>35.65 mm	130 (78.30)	95 (38.00)	5.89 (3.76 – 9.23)				
MS depth	≤35.44 mm	45 (27.10)	145 (58.00)	Referent	<0.001	3.82 (2.48 – 5.87)	<0.001	0.786
	>35.44 mm	121 (72.90)	105 (42.00)	3.71 (2.43 – 5.68)				
MS width	≤26.65 mm	60 (36.10)	141 (56.40)	Referent	<0.001	2.28 (1.52 – 3-43)	<0.001	0.590
	>26.65 mm	106 (63.90)	109 (43.60)	2.29 (1.53 -3.42)				
Diameter of IOF in the axial plane	≤4.15 mm	66 (39.80)	138 (55.20)	Referent	0.002	1.80 (1.21 – 2.70)	0.004	0.881
	>4.15 mm	100 (60.20)	112 (44.80)	1.87 (1.25 – 2.78)				
Diameter of IOF in the sagittal plane	≤3.67 mm	59 (35.50)	140 (56.00)	Referent	<0.001	2.30 (1.53 – 3.46)	<0.001	0.280
	>3.67 mm	107 (64.50)	110 (44.00)	2.31 (1.54 – 3.46)				
Diameter of IOF in the coronal plane	≤3.71 mm	63 (38.00)	146 (58.40)	Referent	<0.001	2.19 (1.46 – 3.28)	<0.001	0.929
	>3.71 mm	103 (62.00)	104 (41.60)	2.30 (1.54 – 3.43)				
Distance from the mid-point of the IOF to the AC	≤29.72 mm	63 (38.00)	126 (50.40)	Referent	0.013	1.67 (1.11 – 2.50)	0.013	0.837
	>29.72 mm	103 (62.00)	124 (49.60)	1.66 (1.11 – 2.48)				
Length of GPC in the sagittal plane	≤35.60 mm	45 (27.10)	140 (56.00)	Referent	<0.001	3.41 (2.22 – 5.22)	<0.001	0.440
	>35.60 mm	121 (72.90)	110 (44.00)	3.42 (2.24 – 5.23)				
Anteroposterior diameter of the GPC in the axial plane	≤5.55 mm	50 (30.10)	153 (61.20)	Referent	<0.001	3.74 (2.44 – 5.72)	<0.001	0.414
	>5.55 mm	116 (69.90)	97 (38.80)	3.66 (2.41 – 5.56)				
Distance from the GPC to the PNS	≤15.78 mm	49 (29.50)	154 (61.60)	Referent	<0.001	4.06 (2.65 – 6.24)	<0.001	0.839
	>15.78 mm	117 (70.50)	96 (38.40)	3.83 (2.52 – 5.83)				
Distance from the GPC to the NPC	≤31.94 mm	66 (39.80)	128 (51.20)	Referent	0.022	1.65 (1.10 – 2.47)	0.015	0.696
	>31.94 mm	100 (60.20)	122 (48.80)	1.59 (1.07 – 2.37)				
Distance from the GPC to the pterygoid hamulus	≤9.25 mm	64 (38.60)	136 (54.40)	Referent	0.002	1.79 (1.19 – 2.69)	0.005	0.994
	>9.25 mm	102 (61.40)	114 (45.60)	1.90 (1.28 – 2.84)				
Distance from the medial wall of GPF to the MMS	≤14.98 mm	121 (72.90)	207 (82.80)	Referent	0.016	1.85 (1.15 – 3.00)	0.012	0.950
	>14.98 mm	45 (27.10)	43 (17.20)	1.79 (1.11 – 2.88)				
Distance from the center of GPF to the AC	≤9.25 mm	45 (27.10)	151 (60.40)	Referent	<0.001	4.10 (2.67 – 629)	<0.001	0.791
	>9.25 mm	121 (72.90)	99 (39.60)	4.10 (2.68 – 6.28)				

Abbreviations: MS, maxillary sinus; IOF, infraorbital foramen; AC, alveolar crest; GPC, greater palatine canal; PNS, posterior nasal spine; NPC, nasopalatine canal; GPF, greater palatine foramen; MMS, midline maxillary suture.

[a]Values are given as n (%) of males and females within each dichotomized parameter according ROC curve analysis. [b]Odds ratio (95% confidence interval). [c]Wald test. [d]Hosmer & Lemeshow goodness-of-fit test.

Table 4. Univariate/multivariate binary logistic regression analyses for association of significant anterior maxilla/upper middle line-related variables with the sex trait adjusting for age and alveolar process status.

Parameters		Cases[a]		Univariate analysis		Multivariate binary logistic regression analysis		Calibration[d]
		Male (n = 83)	Female (n = 125)	Unadjusted OR (95% CI)[b]	P-value[c]	Adjusted OR (95% CI)[b]	P-value[c]	
Length of NPC at sagittal plane	≤11.57 mm	24 (28.90)	77 (61.60)	Referent	<0.001	4.89 (2.55 – 9.36)	<0.001	0.981
	>11.57 mm	59 (71.10)	48 (38.40)	3.94 (2.17 – 7.16)				
Minimum anterior-superior buccal bone thickness	≤6.57 mm	23 (27.70)	76 (60.80)	Referent	<0.001	4.86 (2.53 – 9.34)	<0.001	0.803
	>6.57 mm	60 (72.30)	49 (39.20)	4.05 (2.22 – 7.37)				
Diameter of IF	≤3.60 mm	27 (32.50)	80 (64.00)	Referent	<0.001	4.11 (2.23 – 7.57)	<0.001	0.561
	>3.60 mm	56 (67.50)	45 (36.00)	3.69 (2.05 – 6.63)				

Abbreviations: NPC, nasopalatine canal; IF, incisive foramen
[a]Values are given as n (%) of males and females within each dichotomized parameter according ROC curve analysis. [b]Odds ratio (95% confidence interval). [c]Wald test. [d]Hosmer & Lemeshow goodness-of-fit test.

to the MMS >14.98 mm, and distance from the center of GPF to the AC >9.25 mm. It was further striking that, regarding anterior maxilla/upper middle line-related variables (Table 4), the OR was also significantly increased for male group in cases with a length of NPC at sagittal plane >11.57 mm, minimum anterior-superior buccal bone thickness >6.57 mm, and a diameter of IF >3.60 mm. After adjusting for the effects of confounders, all these candidate variables remained strong and independently associated with the male sex (P <0.05).

DISCUSSION

Detailed study of the maxillary anatomical structures has been helpful in diverse fields, including oral and maxillofacial surgery, otorhinolaryngology, ophthalmology, plastic surgery, head and neck surgery, as well as in forensic and anthropological practices (Ali et al., 2018; Paknahad et al., 2017). As can be appreciated from the references provided, there are many dry-skull- and CBCT-based studies in which anatomical variations of the MS, infraorbital region, hard palate, anterior maxillary region, and their related anatomical structures have been examined separately, but the information has been not only fragmentary, but also the results have been controversial. At the knowledge of the authors, this is the first study, using CBCT scans, that reports comprehensively data concerning the strength/independence of dimensional differences and morphological variations of diverse maxillary structures based on sex comparisons, and taking into account synchronously the modifying effect of the age and alveolar process status on the measurements and observations performed in the sample. Alternatively, this study demonstrated that CBCT imaging is a reliable method for the assessment of morphological and morphometric features of various reference points related with the maxillary bone, as the intra-observer reproducibility values were significantly excellent for the evaluated data in all multiplanar reconstructions. The clinical relevance of the accurate knowledge about the occurrence, exact location, and dimensions of these structures lies in its implication in numerous surgical procedures, including the surgical removal of impacted or supernumerary teeth, or also in orthognathic, implant, periodontal, endodontic, or sinus surgery (Ali et al., 2018; Manzanera et al., 2018; Martins-Júnior et al., 2017; von Arx et al., 2013) among many others, as the inattention of these anatomical variations may lead to surgical failures and/or complications.

It has been acknowledged that male and female cranial structures differ, which is referred as sexual dimorphism (Thornhill and Gangestad, 2006), and that this phenomenon is as great as in other parts of the body (Baughan and Demirjian, 1978).

Considering that estrogen levels limit the growth of facial bones, while testosterone, along with growth hormones, enhance it (Thornhill and Gangestad, 2006), it would be possible to argue that a high ratio of testosterone-to-estrogen might affect the facial growth (Bardin and Catterall, 1981). In agreeance with the former, in this study, the dimensions of the right and left MS were significantly greater in males when compared with those of females. This finding is consistent with those of previous studies (Farias et al., 2019; Kanthem et al., 2015; Paknahad et al., 2017; Sahlstrand-Johnson et al., 2011; Uthman et al., 2011), but differs from other (Genç et al., 2018) in which no sexual dimorphism was identified in relation to these parameters. Moreover, like in this study, some researchers have found no significant differences between the two sides (Farias et al., 2019; Sahlstrand-Johnson et al., 2011), whereas others have documented statistical differences between the right and left MS both in males and females (Uthman et al., 2011). Despite former discrepancies, all resulting data from the MS measurements appear to correspond well with those disclosed by others (Farias et al., 2019; Genç et al., 2018; Kanthem et al., 2015; Paknahad et al., 2017; Sahlstrand-Johnson et al., 2011; Uthman et al., 2011). Overall, these results are especially important considering that both the number and total duration of respiratory infections have been linked negatively with male, but positively with female sex (Thornhill and Gangestad, 2006). Moreover, large national surveys from North America have reported that chronic rhinosinusitis is approximately twice as common in females as in males (Ference et al., 2015). In contrast, the distance from the floor of the sinus to the AC appears not to be influenced by sexual dimorphism or the side of the maxillary segment, but rather by the atrophic/partially atrophic condition of the alveolar crest, which is in line with studies that have shown that the reduced vertical dimension in the posterior maxilla of edentulous individuals is linked to the ridge resorption and the MS pneumatization (Canger and Celenk, 2012; Farina et al., 2011).

Other sinus-related structures analyzed, for which divergent outcomes have been published, were the antral septa and the PSAAC. It has been proposed that, etiologically, antral septa might represent partly congenital abnormalities (primary septa) derived from the developing maxilla or partly acquired abnormalities (secondary septa) related to the irregular atrophy of the posterior maxillary alveolar process (Hungerbühler et el. 2019; Talo Yildirim et al., 2017). In this study, regardless of the origin, a high prevalence of sinus septa, with no significant differences according to sex, age, side, or alveolar process status was detected in the scans, which concurs with some studies (Genç et al., 2018; Talo Yildirim et al., 2017), which have suggested that there is a wide variation in the prevalence of sinus septa, irrespective of the demographic characteristics of the individuals or the degree of alveolar atrophy. On the other hand, the differences in the studies related to the PSAAC are very wide. In the present study, the PSAAC was large enough to be identified by CBCT scans in more than three quarters of the cases, being the intraosseous presentation the most frequently observed (69.11%), followed by the presentation below the sinus membrane (25.80%), and on the outer cortex (5.09%), which is relatively in accordance with the frequencies reported in some studies (Elian et al., 2005; Güncü et al., 2011). Even so, the comparison of detection rates per sex, sides, age category, or alveolar process status did not throw significant differences. Although, these results coincide, at least partially, with those of an earlier study (Genç et al., 2018), andalso differs from others which have reported significantly greater detection rates in females (Güncü et al., 2011) and older adults (Khojastehpour et al., 2016). Moreover, whereas it has been proposed that the diameter and the distance from the artery to the AC are greater in males compared to females (Genç et al., 2018; Güncü et al., 2011; Khojastehpour et al., 2016), the present results failed to show such differences. Notwithstanding, it was noteworthy that this distance was significantly less in cases with atrophic/partially atrophic alveolar process, as has also been described by others (Tehranchi et al., 2017; Velasco-Torres et al., 2016) who postulates that, since variations in the level of the alveolar process depend on the absence of teeth, the height of the residual alveolar crest might be considered as an utmost factor in determining the approximate position of the PSAAC.

Another issue of discussion concerns the sexual dimorphism in the characteristics and morphometric aspects of the infraorbital region, since although it is difficult to compare the results presented herein with other experimental data due to differences in the landmarks used, in consonance with other observations (Bahşi et al., 2019a), this study confirmed, at least in part, that not only the axial, sagittal, and coronal dimensions of IOF, but also the distance from the IOF to the AC, are significantly greater in the male group with no side-related differences. Nevertheless, some authors have failed to identify statistical differences according to sex, though several morphometric parameters have shown higher values in males than in females and significant differences between the left and right sides (Dagistan et al., 2017). Two other important structures evaluated in this region were the Csin and AIOF. With regard to Csin, an important but little-known structure that has a singular tortuous pathway within the anterior wall of the MS below the orbital margin (von Arx et al., 2013), although no significant sex-related differences could be detected, the high detection rate in this study was remarkable and confirms that it should be regarded as a common reference landmark and not an anatomical anomaly of the superior alveolar nerve (Wanzeler et al., 2015). Conversely, the detection rate of the AIOF in the present study, albeit low and showing no significant sex-related differences, was practically analogous to various reported data (Ali et al., 2018; Martins- Júnior et al., 2017), but also dissimilar from that described in other studies (Dagistan et al., 2017; Nanayakkara et al., 2016; Polo et al., 2019) performed on adult dry skulls or CBCT evaluations. In fact, on the basis of its detection frequency some authors believe that the occurrence of AIOF might have a genetic basis (Polo et al., 2019).

The current study also analyzed a series of parameters useful to characterize the GPC in this adult sample. Accordingly, seven specific measurements were significantly higher in the male group, including the length of GPC in the sagittal plane, the anteroposterior diameter of the GPC in the axial plane, the distance from the GPC to the PNS, NPC, and to pterygoid hamulus, as well as the distance of GPF to the MMS and to AC. Although there is great variability in the measurements obtained by other authors, the results obtained in this work indicated a close concordance with the published data (Aoun et al., 2015; Bahşi et al., 2019b; Gibelli et al., 2017, Ikuta et al., 2013; Rapado-González et al., 2015; Tomaszewska et al., 2015). Assuming that age, side, or alveolar process status had no statistical influence on the measurements, all significant sex-related differences detected in various measurements can be also accounted by sexual dimorphism and are consistent with reports of male-female differences of the craniofacial complex (Aoun et al., 2015; Baughan and Demirjian, 1978; Gibelli et al., 2017, Görürgöz and Öztaş, 2022; Tomaszewska et al., 2015). However, discordant data have been also reported regarding these dimorphic traits (Bahşi et al., 2019b; Ikuta et al., 2013; Rapado-González et al., 2015). Another outstanding issue of the herein results was that, in absence of age-, side-, or sex-related differences, a significant greater proportion of GPF located on line with the posterior margin of the PB were observed in cases with atrophic/partially atrophic alveolar process. Although little information is available about this relationship, this finding might be in agreement with a study which suggests that the anteroposterior position of GPF does not depend upon the sex and side (Gibelli et al., 2017); instead, it might actually be related to the decreased alveolar ridge dimensions in maxillary posterior segments of edentulous and partially edentulous individuals (Farina et al., 2011). A further point of agreement between this work and prior investigations (Bahşi et al., 2019b; Gibelli et al., 2017) refers to the lack of significant differences in terms of sex, age, side, and alveolar process status for the number of LPF and for the angle among the horizontal plane of PB and the GPC. Nonetheless, due to the inconstant reported frequency of LPF, but also because the reference points used in this and other works differ from each other, more data would require for determining the variability of this anatomic trait.

The outcome analysis for the anterior maxilla/upper middle line showed differences only for some variables. In terms of sex, the present results were similar to other researches that found

significantly greater measures for the length of NPC (Bornstein et al., 2011; Görürgöz and Öztaş, 2022; Hakbilen and Magat, 2018; Khojastepour et al., 2017; Rai et al., 2021), anterior- superior buccal bone thickness (Bornstein et al., 2011; Hakbilen and Magat, 2018; Khojastepour et al., 2017), and diameter of IF (Bahşi et al., 2019c; Görürgöz and Öztaş, 2022; Khojastepour et al., 2017; Rai et al., 2021) in the male group. Nevertheless, dissenting data have also been reported (Bahşi et al., 2019c; Hakbilen and Magat, 2018). Although the exact reason for differences between men and women is not fully clear, it might be argued that these variations constitute a reflection of hormone-dependent sexually dimorphic traits. At the same time, and in agreement with data that suggest that the NPC is not a static structure but shows dimensional changes liaised with parameters such as aging and tooth loss (Hakbilen and Magat, 2018; Mardinger et al., 2008), the values presented herein for the length of NPC and the buccal bone thickness were significantly smaller in cases with age >50.5 years or atrophic/partially atrophic alveolar process, so that these measurements might related to bone remodeling and increased structural loss observed with age progression (Hakbilen and Magat, 2018). It is important to highlight that the current results might parallel, at least partially, those described by other studies (Bahşi et al., 2019c; Görürgöz and Öztaş, 2022; Hakbilen and Magat, 2018; Jayasinghe et al., 2020), which found that the age, sex, or alveolar process status had no significant effects on the number of nasal/buccal openings, angulation, or shapes of the NPC. In this sense, it has been concluded that the morphology of the NPC is highly variable and different populations show diverse traits/shapes (Görürgöz and Öztaş, 2022; Jayasinghe et al., 2020). Another investigated subject was the maturation of the MPS, in which regardless of the sex or alveolar process status, stage E was found to be significantly more frequent in cases aged >50.5 years. Whereas there is no available information pertaining to the maturation of facial sutures in adulthood, this finding concurs with evidence that stage E increases in prevalence with age (Angelieri et al., 2017). Inasmuch as the continuous progress of skeletal maturation can lead to the obliteration of the MPS (Reis et al., 2020), the age of the individuals may be a practical alternative to predict some MPS stages (Angelieri et al., 2015). The last topic evaluated in this work included the detection of incidental findings on both sides of the posterior maxillary region and on the anterior maxilla/upper middle line. The results showed a low frequency of these alterations, the most common being torus palatinus (11.10%), followed by palatal/buccal exostoses (6.00%), and just a small number of cases of idiopathic osteosclerosis (1.00%). Considering that no significant differences were detectable between the proportions observed according to sex, age, side, or alveolar process status, these detection rates were close similar to those already reported for maxillary CBCT scans (Lopes et al., 2017; Price et al., 2012). Despite the low detection frequency, since these abnormalities can arise anywhere regardless of the sex, age group or alveolar process status, its recognition emphasizes the need to fully examine the volume of the CBCT study to detect the presence of hidden disturbances that may require intervention or monitoring (Price et al., 2012).

It is important to point here that the differences observed between the studies may be attributable to several factors related with the variation in anthropometric characteristics of the sample population, ethnic variability of anatomical structures (Ali et al., 2018; Bahşi et al., 2019c; Gibelli et al., 2017; Görürgöz and Öztaş, 2022; Hakbilen and Magat, 2018; Manzanera et al., 2018; Tomaszewska et al., 2015), age groups analyzed (Hakbilen and Magat, 2018; Talo Yildirim et al., 2017), alongside some features related with the methodological heterogeneity, among these, sample size (Hakbilen and Magat, 2018; Jayasinghe et al., 2020), type of image examination (Khojastehpour et al., 2016; Talo Yildirim et al., 2017), measurement techniques, and different anatomical landmarks (Görürgöz and Öztaş, 2022; Jayasinghe et al., 2020; Velasco-Torres et al., 2016). Despite of aforesaid, it has been accepted that although the collected information can vary according to different populations, the outcomes concerning the possible influence of the sex on each parameter are almost unanimously concordant, when stud-

ies are performed according to the same anatomical landmarks (Gibelli et al., 2019). Adding to the former findings, in the present study a total of 14 covariates related to the maxillary posterior region and three covariates related to the maxillary anterior/upper midline were strongly and independently associated with the male sex even after adjusting for age and alveolar process status. This finding is important mainly because, in addition to the fact that these variables may be usefulness for defining safe surgical areas during the planning of different maxillofacial surgical approaches, taking altogether, the CBCT measurements might constitute useful features for sexing of skeletal remains in the forensic or anthropology context when other methods of identification have been inconclusive (Kanthem et al., 2015; Uthman et al., 2011). Hence, additional studies with different statistical approaches using discriminant analyses to investigate different populations are essential to confirm and validate the results obtained in the present study.

As a final point, two main limitations were identified in this study. First, CBCT assessments were performed in a Colombian population that possesses a complex ethnic structure of individuals of different ethnic origins. This fact may preclude the generalizability of the study outcomes to other ethnic groups with different maxillary morphological features. Second, although overall the increased values of 17 covariates were strongly and independently associated with the male sex, other parameters, including the chewing function, extent of tooth loss, and the period of wearing prosthesis might have an important effect on the reported data. Even so, since to transfer the results to clinically relevant conditions, the findings must be strong and constant across different comparisons, adhering to the outcomes presented, it appears that, regardless of dental and prosthetic features, all of these covariates are robustly linked to the male sex.

CONCLUSION

Based on the current data, it would possible to conclude that the maxillary bone can present several morphological variations, as well as dimensional differences that may be strongly liaised to sex but are independent of age, side, and the state of the alveolar process of the population observed. Even so, both aging and alveolar process status should be considered when applying the anatomical variation data to the needs of the particular case.

ACKNOWLEDGEMENTS

This study has been supported by the Technical Research Council of the Faculty of Dentistry of University of Antioquia (CIFO-Code 2021-40871). Special thanks to RADEX 3D Specialized Radiology Center, Medellín, Colombia for providing CBCT scans.

REFERENCES

ALI IK, SANSARE K, KARJODKAR FR, SALVE P (2018) Cone beam computed tomography assessment of accessory infraorbital foramen and determination of infraorbital foramen position. *J Craniofac Surg,* 29(2): e124-e126.

ANGELIERI F, CEVIDANES LH, FRANCHI L, GONÇALVES JR, BENAVIDES E, MCNAMARA JA JR (2013) Midpalatal suture maturation: classification method for individual assessment before rapid maxillary expansion. *Am J Orthod Dentofacial Orthop,* 144(5): 759-769.

ANGELIERI F, FRANCHI L, CEVIDANES LH, MCNAMARA JA JR (2015) Diagnostic performance of skeletal maturity for the assessment of midpalatal suture maturation. *Am J Orthod Dentofacial Orthop,* 148(6): 1010-1016.

ANGELIERI F, FRANCHI L, CEVIDANES LHS, GONÇALVES JR, NIERI M, WOLFORD LM, MCNAMARA JA JR (2017) Cone beam computed tomography evaluation of midpalatal suture maturation in adults. *Int J Oral Maxillofac Surg,* 46(12): 1557-1561.

AOUN G, NASSEH I, SOKHN S, SAADEH M (2015) Analysis of the greater palatine foramen in a Lebanese population using cone-beam computed tomography technology. *J Int Soc Prev Community Dent,* 5 (Suppl 2): S82-S88.

BAHŞI I, ORHAN M, KERVANCIOĞLU P, YALÇIN ED (2019a) Morphometric evaluation and surgical implications of the infraorbital groove, canal and foramen on cone-beam computed tomography and a review of literature. *Folia Morphol (Warsz),* 78(2): 331- 343.

BAHŞI İ, ORHAN M, KERVANCIOĞLU P, YALÇIN ED (2019b) Morphometric evaluation and clinical implications of the greater palatine foramen, greater palatine canal and pterygopalatine fossa on CBCT images and review of literature. *Surg Radiol Anat*, 41(5): 551-567.

BAHŞI I, ORHAN M, KERVANCIOĞLU P, YALÇIN ED, AKTAN AM (2019c) Anatomical evaluation of nasopalatine canal on cone beam computed tomography images. *Folia Morphol (Warsz)*, 78(1): 153-162.

BARDIN CW, CATTERALL JF (1981) Testosterone: a major determinant of extragenital sexual dimorphism. *Science*, 211(4488): 1285-1294.

BAUGHAN B, DEMIRJIAN A (1978) Sexual dimorphism in the growth of the cranium. *Am J Phys Anthropol,* 49 (3): 383-390.

BORNSTEIN MM, BALSIGER R, SENDI P, VON ARX T (2011) Morphology of the nasopalatine canal and dental implant surgery: a radiographic analysis of 100 consecutive patients using limited cone-beam computed tomography. *Clin Oral Implants Res*, 22(3): 295-301.

CANGER EM, CELENK P (2012) Radiographic evaluation of alveolar ridge heights of dentate and edentulous patients. *Gerodontology*, 29(1): 17-23.

DAGISTAN S, MILOĞLU Ö, ALTUN O, UMAR EK (2017) Retrospective morphometric analysis of the infraorbital foramen with cone beam computed tomography. *Niger J Clin Pract*, 20(9): 1053-1064.

ELIAN N, WALLACE S, CHO SC, JALBOUT ZN, FROUM S (2005) Distribution of the maxillary artery as it relates to sinus floor augmentation. *Int J Oral Maxillofac Implants*, 20(5): 784-787.

FARIAS GOMES A, DE OLIVEIRA GAMBA T, YAMASAKI MC, GROPPO FC, HAITER NETO F, POSSOBON RF (2019) Development and validation of a formula based on maxillary sinus measurements as a tool for sex estimation: a cone beam computed tomography study. *Int J Legal Med*, 133(4): 1241-1249.

FARINA R, PRAMSTRALLER M, FRANCESCHETTI G, PRAMSTRALLER C, TROMBELLI L (2011) Alveolar ridge dimensions in maxillary posterior sextants: a retrospective comparative study of dentate and edentulous sites using computerized tomography data. *Clin Oral Implants Res*, 22(10): 1138-1144.

FERENCE EH, TAN BK, HULSE KE, CHANDRA RK, SMITH SB, KERN RC, CONLEY DB, SMITH SS (2015) Commentary on gender differences in prevalence, treatment, and quality of life of patients with chronic rhinosinusitis. *Allergy Rhinol (Providence)*, 6(2):82-88.

GENÇ T, DURUEL O, KUTLU HB, DURSUN E, KARABULUT E, TÖZÜM TF (2018) valuation of anatomical structures and variations in the maxilla and the mandible before dental implant treatment. *Dent Med Probl*, 55(3): 233-240.

GIBELLI D, BORLANDO A, DOLCI C, PUCCIARELLI V, CATTANEO C, SFORZA C (2017) Anatomical characteristics of greater palatine foramen: a novel point of view. *Surg Radiol Anat*, 39(12): 1359-1368.

GIBELLI D, BORLANDO A, BARNI L, SARTORI P, CAPPELLA A, PUCCIARELLI V, CATTANEO C, SFORZA C (2019) Anatomy of infraorbital foramen: influence of sex, side, and cranium size. *J Craniofac Surg*, 30(4): 1284-1288.

GÖRÜRGÖZ C, ÖZTAŞ B (2021) Anatomic characteristics and dimensions of the nasopalatine canal: a radiographic study using cone-beam computed tomography. *Folia Morphol (Warsz)*, 80(4): 923-934.

GÜNCÜ GN, YILDIRIM YD, WANG HL, TÖZÜM TF (2011) Location of posterior superior alveolar artery and evaluation of maxillary sinus anatomy with computerized tomography: a clinical study. *Clin Oral Implants Res*, 22(10): 1164-1167.

HAKBILEN S, MAGAT G (2018) Evaluation of anatomical and morphological characteristics of the nasopalatine canal in a Turkish population by cone beam computed tomography. *Folia Morphol (Warsz)*, 77(3): 527-535.

HUNGERBÜHLER A, ROSTETTER C, LÜBBERS HT, RÜCKER M, STADLINGER B (2019) Anatomical characteristics of maxillary sinus septa visualized by cone beam computed tomography. *Int J Oral Maxillofac Surg*, 48(3): 382-387.

IKUTA CR, CARDOSO CL, FERREIRA-JÚNIOR O, LAURIS JR, SOUZA PH, RUBIRA-BULLEN IR (2013) Position of the greater palatine foramen: an anatomical study through cone beam computed tomography images. *Surg Radiol Anat*, 35(9): 837-842.

JAYASINGHE RM, HETTIARACHCHI PVKS, FONSEKA MCN, NANAYAKKARA D, JAYASIGHE RD (2020) Morphometric analysis of nasopalatine foramen in Sri Lankan population using CBCT. *J Oral Biol Craniofac Res*, 10(2): 238-240.

KANTHEM RK, GUTTIKONDA VR, YELURI S, KUMARI G (2015) Sex determination using maxillary sinus. *J Forensic Dent Sci*, 7(2): 163-167.

KHOJASTEHPOUR L, DEHBOZORGI M, TABRIZI R, ESFANDNIA S (2016) Evaluating the anatomical location of the posterior superior alveolar artery in cone beam computed tomography images. *Int J Oral Maxillofac Surg*, 45(3): 354-358.

KHOJASTEPOUR L, HAGHNEGAHDAR A, KESHTKAR M (2017) Morphology and dimensions of nasopalatine canal: a radiographic analysis using cone beam computed tomography. *J Dent (Shiraz)*, 18(4): 244-250.

LOPES IA, TUCUNDUVA RM, HANDEM RH, CAPELOZZA AL (2017) Study of the frequency and location of incidental findings of the maxillofacial region in different fields of view in CBCT scans. *Dentomaxillofac Radiol*, 46(1): 20160215.

MANZANERA E, LLORCA P, MANZANERA D, GARCÍA-SANZ V, SADA V, PAREDES-GALLARDO V (2018) Anatomical study of the maxillary tuberosity using cone beam computed tomography. *Oral Radiol*, 34(1): 56-65.

MARDINGER O, NAMANI-SADAN N, CHAUSHU G, SCHWARTZ-ARAD D (2008) Morphologic changes of the nasopalatine canal related to dental implantation: a radiologic study in different degrees of absorbed maxillae. *J Periodontol*, 79(9): 1659-1662.

MARTINS-JÚNIOR PA, RODRIGUES CP, DE MARIA ML, NOGUEIRA LM, SILVA JH, SILVA MR (2017) Analysis of anatomical characteristics and morphometric aspects of infraorbital and accessory infraorbital foramina. *J Craniofac Surg*, 28(2): 528-533.

NANAYAKKARA D, PEIRIS R, MANNAPPERUMA N, VADYSINGHE A (2016) Morphometric analysis of the infraorbital foramen: the clinical relevance. *Anat Res Int,* 2016: 7917343.

PAKNAHAD M, SHAHIDI S, ZAREI Z (2017) Sexual dimorphism of maxillary sinus dimensions using cone-beam computed tomography. *J Forensic Sci*, 62(2): 395-398.

POLO CL, ABDELKARIM AZ, VON ARX T, LOZANOFF S (2019) The morphology of the infraorbital nerve and foramen in the presence of an accessory infraorbital foramen. *J Craniofac Surg*, 30(1): 244-253.

PRICE JB, THAW KL, TYNDALL DA, LUDLOW JB, PADILLA RJ (2012) Incidental findings from cone beam computed tomography of the maxillofacial region: a descriptive retrospective study. *Clin Oral Implants Res*, 23(11): 1261-1268.

RAI S, MISRA D, MISRA A, KHATRI M, KIDWAI S, BISLA S, JAIN P (2021) Significance of morphometric and anatomic variations of nasopalatine canal on cone-beam computed tomography in anterior functional zone - a retrospective study. *Ann Maxillofac Surg*, 11(1): 108-114.

RAPADO-GONZÁLEZ O, SUÁREZ-QUINTANILLA JA, OTERO-CEPEDA XL, FERNÁNDEZ-ALONSO A, SUÁREZ-CUNQUEIRO MM (2015) Morphometric study of the greater palatine canal: cone-beam computed tomography. *Surg Radiol Anat*, 37(10): 1217-1224.

REIS LG, RIBEIRO RA, VITRAL RWF, REIS HN, DEVITO KL (2020) Classification of the midpalatal suture maturation in individuals older than 15 years: a cone beam computed tomographic study. *Surg Radiol Anat*, 42(9): 1043-1049.

SAHLSTRAND-JOHNSON P, JANNERT M, STRÖMBECK A, ABUL-KASIM K (2011) Computed tomography measurements of different dimensions of maxillary and frontal sinuses. *BMC Med Imaging*, 11: 8.

TALO YILDIRIM T, GÜNCÜ GN, COLAK M, NARES S, TÖZÜM TF (2017) Evaluation of maxillary sinus septa: a retrospective clinical study with cone beam computerized tomography (CBCT). *Eur Rev Med Pharmacol Sci*, 21(23): 5306-5314.

TEHRANCHI M, TALEGHANI F, SHAHAB S, NOURI A (2017) Prevalence and location of the posterior superior alveolar artery using cone-beam computed tomography. *Imaging Sci Dent*, 47(1): 39-44.

THORNHILL R, GANGESTAD SW (2006) Facial sexual dimorphism, developmental stability, and susceptibility to disease in men and women. *Evol Hum Behav*, 27(2): 131-144.

TOMASZEWSKA IM, KMIOTEK EK, PENA IZ, ŚREDNIAWA M, CZYŻOWSKA K, CHRZAN R, NOWAKOWSKI M, WALOCHA JA (2015) Computed tomography morphometric analysis of the greater palatine canal: a study of 1,500 head CT scans and a systematic review of literature. *Anat Sci Int,* 90(4): 287-297.

UTHMAN AT, AL-RAWI NH, AL-NAAIMI AS, AL-TIMIMI JF (2011) Evaluation of maxillary sinus dimensions in gender determination using helical CT scanning. *J Forensic Sci*, 56(2): 403-408.

VELASCO-TORRES M, PADIAL-MOLINA M, ALARCÓN JA, O´VALLE F, CATENA A, GALINDO-MORENO P (2016) Maxillary sinus dimensions with respect to the posterior superior alveolar artery decrease with tooth loss. *Implant Dent*, 25(4): 464-470.

VON ARX T, LOZANOFF S, SENDI P, BORNSTEIN MM (2013) Assessment of bone channels other than the nasopalatine canal in the anterior maxilla using limited cone beam computed tomography. *Surg Radiol Anat*, 35(9):783-790.

WANZELER AM, MARINHO CG, ALVES JUNIOR SM, MANZI FR, TUJI FM (2015) Anatomical study of the canalis sinuosus in 100 cone beam computed tomography examinations. *Oral Maxillofac Surg*, 19(1):49-53.